Controlling Bond Scission Pathways of Isopropanol on Fe- and Pt-Modified Mo_2N Model Surfaces and Powder Catalysts

*William N. Porter[1], Hilda A. Mera[2], Wenjie Liao[3], Zhexi Lin[1], Ping Liu[3], John R. Kitchin[2], Jingguang G. Chen[1,3]**

[1] Department of Chemical Engineering, Columbia University, New York, NY 10027, USA

[2] Department of Chemical Engineering, Carnegie Mellon University, Pittsburgh, PA 15213, USA

[3] Chemistry Division, Brookhaven National Laboratory, Upton, New York 11973, USA

* Corresponding author: jgchen@columbia.edu

Keywords*: molybdenum nitride, isopropanol, dehydrogenation, dehydration, biomass, surface science*

Abstract

Biomass valorization can be used to produce value-added chemicals and fuels from renewable biomass resources by upgrading them via selective bond scission while retaining certain functional groups. Specifically, upgrading biomass through the dehydrogenation of alcohols to carbonyl compounds has gained interest as a method of utilizing biomass-derived alcohols while additionally producing H_2. In this work, isopropanol was used as a probe molecule to control bond scission selectivity over Fe- and Pt-modified molybdenum nitride (Mo_2N) model surfaces and powder catalysts. Trends in the selectivity toward dehydration and dehydrogenation were dependent on both the type and coverage of the metal overlayer on model surfaces. These results were then extended to the corresponding powder catalysts to demonstrate how model surface studies can inform the design of supported catalysts. Density functional theory calculations provided insights into controlling the dehydration and dehydrogenation pathways. This work shows that fundamental understanding of the reactivity and intermediates on Mo_2N-based model surfaces

can be applied to understand the catalytic performance of metal-modified Mo_2N powder catalysts, as well as demonstrates that Mo_2N-based catalysts are potentially promising materials for upgrading biomass-derived oxygenates.

1. Introduction

Biomass valorization is a promising method to produce commodity chemicals from renewable biomass resources. Due to the presence of multiple functionalities in biomass molecules, upgrading them requires breaking certain bonds while retaining the functional groups of interest.[1] Many processes of converting lignocellulosic biomass into useful fuels and chemicals involve selective bond scission steps: from C−O cleavage during hydrodeoxygenation of bio-oil[2] to selectively breaking C−C or C−O bonds of biomass-derived oxygenates.[3–5] Thus, one of the fundamental challenges of commercializing these processes is in effectively controlling these pathways. Among the various upgrading reactions, which include dehydrogenation,[6,7] hydrodeoxygenation,[8] hydrolysis[9] and dehydration,[10] the dehydrogenation of alcohols to carbonyl compounds has recently gained interest as a method of producing biomass-derived alcohols and H_2. A recent study of a variety of transition metal alloys, nitrides, and carbides has identified Mo_2N as a promising material for this reaction,[11] and other work has shown dehydration/dehydrogenation of formic acid on bulk and nitrogen-doped carbon-supported Mo_2N.[12] Furthermore, modifying Mo_2N with metals is a potentially promising way to control bond scission reactions of simple oxygenates including reforming of ethanol on Pt/Mo_2N [13] and dehydration of glycerol on Cu/Mo_2N.[8] Additionally, strong metal-support interactions between Co and Mo_2N have been demonstrated for CO_2 hydrogenation.[14] Despite the promising catalytic properties of Mo_2N-based catalysts, there is insufficient fundamental understanding of the trends in selective conversion of oxygenates that emerge when different transition metals are added to Mo_2N. Thus, it is critical to elucidate the nature of the synergy between the admetals and the Mo_2N surface.

In this work, we investigated well-characterized Fe- and Pt-modified Mo_2N surfaces toward C−O, C−C, and C−H bond scission using isopropanol as a probe molecule. The reaction pathways were identified using temperature programmed desorption (TPD) and high-resolution electron energy loss spectroscopy (HREELS) under

ultrahigh vacuum (UHV) conditions. Trends in the selectivity toward decomposition, dehydration, and dehydrogenation were dependent on both the type and coverage of the metal overlayer on Mo_2N surfaces. Unmodified Mo_2N favored C−O cleavage (dehydration) to form propylene, and the addition of Fe and Pt both decreased the activity toward dehydration. Of the partially covered metal-modified surfaces, Pt/Mo_2N showed the highest dehydrogenation activity to produce acetone, while on Fe/Mo_2N, the C−H scission activity did not increase until the Fe coverage grew above one monolayer (ML). The amount of isopropanol undergoing reactions was the lowest on unmodified Mo_2N, followed by Fe/Mo_2N, with Pt/Mo_2N displaying the highest activity. Vibrational studies using HREELS were performed to characterize surface species during the reaction and density functional theory (DFT) calculations provided insights into the reaction pathways. The trends in activity and selectivity over model surfaces were then extended to the corresponding powder catalysts. The trend in the initial production rate of C_3 products agreed well with the total activity observed on the model surfaces. In terms of selectivity, Mo_2N had the highest ratio of dehydration to dehydrogenation, and this ratio decreased upon addition of Fe and Pt, in agreement with the model surface results. This work shows that fundamental understanding on model surfaces can be used to understand trends in activity and selectivity of powder catalysts, and that Fe- and Pt-modified Mo_2N catalysts show promise for selectively upgrading biomass-derived oxygenates.

2. Methods Section

2.1. Model surface studies in ultrahigh vacuum

Two separate UHV chambers with base pressures of approximately 5×10^{-10} Torr were employed to perform TPD and HREELS experiments. A polycrystalline Mo_2N film was mounted to two Ta posts for resistive heating and liquid N_2 cooling. The temperature was monitored using a K-type thermocouple welded to the back of the film. The film was cleaned using cycles of ion sputtering and annealing, and Fe and Pt overlayers were deposited through physical vapor deposition. Auger electron spectroscopy (AES) was used to monitor the overlayer coverage, and a layer-by-layer growth mechanism was confirmed by the presence of a break in the Fe and Pt growth curves (Figure S1). The TPD experiments were conducted using a mass spectrometer (MS, Hiden HAL 3F-RC) to monitor the

species desorbing as the surface was heated at a rate of 3 K/s. Activity was quantified by comparing the peak area to the H_2 desorption peak corresponding to a known C coverage determined by AES from an ethylene decomposition TPD, as detailed in the SI. Mass spectrometry sensitivity factors were used to normalize the peak area for each product. The HREEL spectra were obtained using an LK3000 spectrometer, as described in detail elsewhere.[15]

The Mo_2N film was synthesized using polycrystalline Mo foil (Alfa Aesar, 99.95%) in a procedure that has been reported previously.[8] In brief, the foils were cleaned via sonication in ethanol before nitridation in a tube furnace. Under pure ammonia gas (150 ml/min), the temperature was increased at a rate of 7 K/min up to 1123 K, and then held for 10 hours before cooling back to room temperature. The synthesized Mo_2N foils were then characterized using XRD and GI-XRD to confirm the presence of surface Mo_2N.

2.2. Powder catalyst evaluation at ambient pressure

The Mo_2N powders were synthesized using a procedure starting with an ammonium paramolybdate ($(NH_4)_6Mo_7O_{24})\cdot 4H_2O$, Alfa Aesar, 99%) precursor. The precursor was first calcined at 773 K for 4 h to produce MoO_3, which was then transferred to a quartz tube furnace and nitrided by ramping at 5 K/min up to 923 K and holding for 2 h under ammonia gas (200 ml/min). XRD was used to confirm the presence of γ-Mo_2N. The Fe- and Pt-modified Mo_2N were synthesized via incipient wetness impregnation of aqueous solutions of metal precursors ($Fe(NO_3)_3\cdot 9H_2O$, Alfa Aesar, 99.999% and $Pt(NH_3)_4(NO_3)_2$, Alfa Aesar, 99.99%). To compare equivalent atomic fractions, weight loadings of 1.4 wt% Fe/Mo_2N and 5 wt% Pt/Mo_2N were used. CO chemisorption measurements of the reduced powders were conducted in an Altamira AMI-300ip using pulses of 10% CO at 40 °C. The prepared catalysts were loaded into a vertical quartz tube furnace, and reduced at 863 K for 2 hours in 20 ml/min of N_2/H_2 (1:3). The reactor was then cooled to the reaction temperature (413 K or 473 K) in the H_2/N_2 flow, and purged with Ar before starting a reaction. Isopropanol was introduced by a flow of Ar (10 ml/min) through a bubbler, and the products were analyzed using a gas chromatograph equipped with PoraPLOT Q and Mol Sieve columns.

For the steady-state analysis of selectivity, 40 mg of Mo_2N and Fe/Mo_2N, and 20 mg of Pt/Mo_2N:SiO_2 (1:6) were loaded into the reactor. A temperature of 413 K was used to achieve conversion ranging from 1–2% in order

to minimize transport effects. An average of the steady-state flow rates from 8–12 h was used to calculate the selectivity of product j (S_j), based on the flow rate of product j (F_j), according to:

$$S_j = \frac{F_{j,out}}{\sum F_{j,out}} \quad (1)$$

For the comparison of conversion, loadings of 40 mg of Mo_2N and Fe/Mo_2N, and 20 mg Pt/Mo_2N were used. The temperature was held at 473 K. Conversion of isopropanol (X_{IPA}), was calculated using the total flow rate of products ($\sum F_{j,out}$) and the feed flow of isopropanol ($F_{IPA,in}$), as:

$$X_{IPA} = \frac{\sum F_{j,out}}{F_{IPA,in}} \quad (2)$$

2.3. XANES measurements

In-situ XANES measurements were performed at the 7-BM beamline of the National Synchrotron Light Source II (NSLS-II), Brookhaven National Laboratory (BNL). For each experiment, 100 mg of catalyst was pressed into a 13 mm pellet that was loaded into a Nashner-Adler cell. The reduction was performed by heating to 823 K in 15 ml/min N_2/H_2 (3:1) and holding until the spectra stabilized. The catalyst was then cooled to 473 K and isopropanol was introduced using a bubbler, similar to conditions used in the flow reactor experiments. The Fe K-edge and Pt L_3-edge spectra were collected using a total fluorescence yield detector.

2.4. DFT calculations

Spin-polarized DFT calculations were performed using the Perdew-Burke-Ernzerhof (PBE) type of exchange-correlation functional[16] and projector augmented wave (PAW) pseudopotential implemented in the Vienna *ab initio* Simulation Package (VASP).[17–21] Valence electron wavefunctions were represented using a plane wave basis set in periodic boundary conditions, with a kinetic energy cutoff at 500 eV. For the electronic relaxation, the Brillouin zone integration was performed on a Γ-centered 3×3×1 k-point mesh grid with 5 irreducible k-points. The Gaussian smearing method was used with k_BT = 0.05 eV, which was later extrapolated to k_BT = 0 eV to get the exact total energy. The convergence threshold for the total energy variance during electronic relaxation was set to 10^{-5} eV. For the ionic relaxation, the conjugate-gradient algorithm was used to relax the ions until the maximum

norm of atomic forces felt by each atom was less than 0.01 eV/Å. The DFT-calculated binding energy of atomic oxygen (*O) was defined by equation 3. The van der Waals interactions were not included in current DFT calculations. In a case study of acetone adsorption on $Mo_2N(111)$ and $Pt/Mo_2N(111)$, the adsorption energy calculated using DFT without incorporating Grimme's D3 dispersion correction[22] was found to describe the adsorption enthalpy determined by TPD better than that using DFT-D3 (Table S5). Therefore, dispersion corrections were not included in the current study.

$$\mathrm{BE(O)} = \mathrm{E(^{*}O/surface)} - \frac{1}{2}\mathrm{E}\left(\mathrm{O_2(g)}\right) - \mathrm{E(surface)} \quad (3)$$

The N-terminated γ-$Mo_2N(111)$ surface was selected as the model surface for the polycrystalline Mo_2N film due to its prior identification as the thermodynamically most stable surface of Mo_2N.[23] Using previous research as a guide,[24] the Mo_2N bulk structure was built by removing 50% of nitrogen atoms from the fcc MoN structure in the 100/010 direction. Upon the geometry optimization, the bulk Mo_2N structure adhered to a tetragonal lattice with lattice vectors a=b=4.21 Å and c=4.17 Å. Notably, these values closely match the experimentally determined lattice constant of 4.16 Å as measured by XRD.[25] The optimized Mo_2N bulk structure was subsequently cleaved to the N-terminated γ-$Mo_2N(111)$ – p(4×4) surface with 7 atomic layers (Figure S7a). This slab model spans dimensions of 11.86 Å × 11.86 Å × 22.27 Å and includes a 15 Å vacuum layer set perpendicular to the (111) facet. To model the Pt-modified $Mo_2N(111)$ surface, a monolayer coverage of Pt was deposited onto the $Mo_2N(111)$ surface. The resulting average Pt-Pt bond length within the Pt overlayer (2.74 Å, Figure S7b) is very similar to that of Pt(111) (2.76 Å).

3. Results and Discussion

3.1. Experimental studies of isopropanol on model surfaces

3.1.1. Bond scission pathways determined using TPD

To probe the effect of metal modifiers on the Mo_2N surface, isopropanol TPD experiments on unmodified Mo_2N and four different coverages of Fe and Pt overlayers were performed. For each experiment, 0.5 L of isopropanol was exposed to the surface at 170 K. The TPD curves showing desorption of CO (28 amu), propylene

(39 amu) and acetone (58 amu) from Mo_2N and near-ML coverages of Fe and Pt on Mo_2N are displayed in Figure 1. Scheme 1 shows the bond scission pathways leading to these three products, and Table 1 summarizes the activity, which was quantified on a per surface site basis. Sensitivity factors for H_2, CO, propylene, and acetone were used to normalize the MS intensity. By comparing the TPD curves of Mo_2N, Fe/Mo_2N and Pt/Mo_2N, the effect of each metal can be elucidated.

The main reaction pathway on Mo_2N was propylene formation, along with minor amounts of acetone and negligible CO production. The CO peak at 319 K (Figure 1a) was attributed mainly to background CO adsorption, which was observed in a blank TPD on the unmodified Mo_2N surface (Figure S2). Unmodified Mo_2N displayed the highest selectivity toward propylene out of all the surfaces studied, with a selectivity of 59%, but the lowest total activity toward all three products (0.016 ML). The propylene (Figure 1b) and acetone (Figure 1c) peaks were centered at 443 K and 430 K, with onset temperatures of 270 K and 360 K, respectively. The observation of propylene production was consistent with a previous study showing selective C−O bond scission activity on Mo_2N from the dehydration of glycerol.[8] The addition of Fe and Pt overlayers both decreased propylene production, but led to differing effects on the decomposition and dehydrogenation pathways.

Scheme 1. The bond scission pathways of isopropanol observed on Mo_2N and metal-modified Mo_2N surfaces.

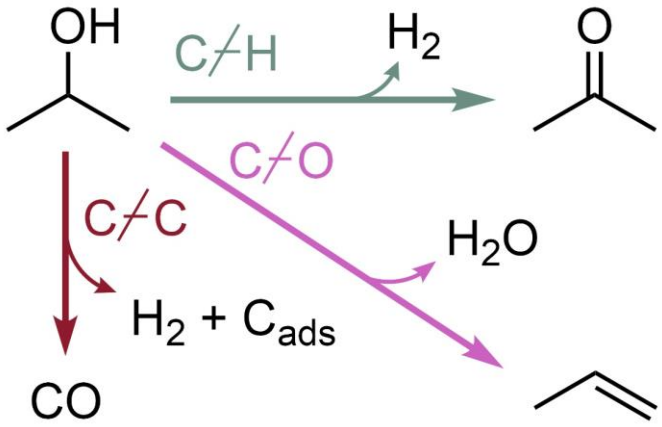

The near-ML Fe/Mo_2N surface led to C−O and C−H scissions, as indicated by the observation of propylene and acetone desorption peaks, respectively, both centered at 416 K. Compared with Mo_2N, the propylene peak from 1.1 ML Fe/Mo_2N was smaller and centered at a lower temperature, while the acetone peak was more intense. The highest acetone selectivity among the Fe/Mo_2N surfaces was 79.9% on 2.0 ML Fe. This result suggested that active sites containing multiple adjacent Fe atoms were likely necessary for C−H bond scission of isopropanol. In addition, C−C bond scission was indicated by the observation of a relatively large CO peak centered at 370 K. The quantified activity in Table 1 showed an interfacial effect of rising CO activity as the coverage was increased up to 0.7 ML, but upon depositing higher Fe coverages of 1.1 and 2.0 ML, this C−C scission activity was attenuated and an increase in activity toward acetone formation was observed.

The 1.3 ML Pt/Mo_2N surface also facilitated the three pathways of C−O, C−H, and C−C scission, but with changes in the peak shape and temperature compared to Mo_2N and Fe/Mo_2N, indicating differences in the reaction mechanism. There was a further decrease in propylene formation activity compared with Fe, as shown by the smaller propylene peak centered at 366 K. The lower temperature 39 amu peak was attributed to acetone fragmentation. On the other hand, Pt/Mo_2N facilitated more acetone formation than both Mo_2N and Fe/Mo_2N, as observed by the larger peak in Figure 1c, which was centered at 284 K on the partially covered Pt surface. This was 146 K lower than the acetone peak temperature on Mo_2N, indicating that interactions between Pt and Mo_2N led to more facile dehydrogenation of isopropanol. Comparing the Pt-modified surfaces in Table 1, the highest dehydrogenation activity of 0.017 ML was observed on the near-ML Pt surface, further suggesting the presence of beneficial interactions between Pt and Mo_2N. A significant amount of C−C scission was also observed based on a CO peak centered at 440 K that was larger and at a higher temperature than 1.1 ML Fe/Mo_2N. CO activity reached a maximum of 0.072 ML on the 2.1 ML Pt/Mo_2N surface. This increase in C−C scission was consistent with previously shown high ethanol reforming activity of Pt/Mo_2N.[13] Of all the surfaces studied, 2.1 ML Pt/Mo_2N displayed the highest total activity (0.088 ML) toward the reaction of isopropanol.

Overall, TPD results revealed three different pathways for the reaction of isopropanol, with trends in the activity dependent on both the type and coverage of the metal overlayer. Mo_2N favored dehydration, and the

addition of Fe and Pt led to a decrease in propylene production. Fe/Mo_2N showed an interfacial preference for C−C cleavage, but was more selective toward acetone at higher Fe coverages. Comparing the partially covered and near-ML surfaces (Figure 1d), higher C−H scission was observed on Pt/Mo_2N than on Fe/Mo_2N. These results suggested that the bond scission pathways can be tuned by varying the type and coverage of metal modifiers on Mo_2N.

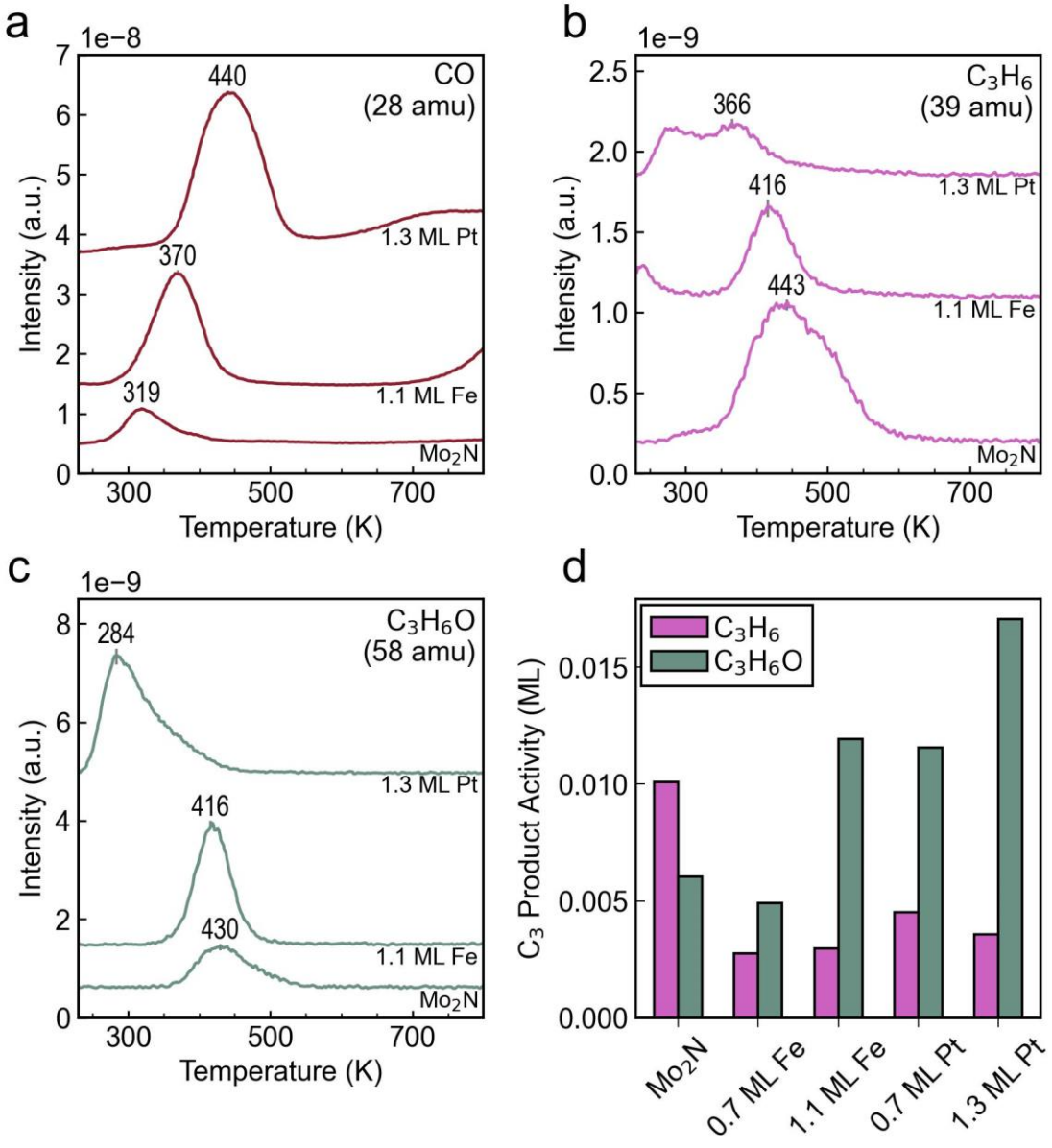

Figure 1. TPD curves after exposing the indicated surfaces to 0.5 L isopropanol at 170 K showing desorption of: (a) carbon monoxide, (b) propylene, and (c) acetone. The mass signal used for each is shown in parentheses. (d) Activity toward the formation of the C_3 products, propylene (pink) and acetone (teal), on partially covered and near-ML surfaces calculated from TPD peak area. The complete set of activity and selectivity data for all of the surfaces tested is shown in Table 1.

Table 1. Quantification of isopropanol reaction pathways on model surfaces

	Activity in ML (Selectivity in %)			
Surface	**CO**	**Propylene**	**Acetone**	**Total**
Mo_2N	0.000 (0.0%)	0.010 (58.8%)	0.006 (35.3%)	0.016
0.4 ML Fe/Mo_2N	0.013 (57.5%)	0.004 (16.7%)	0.006 (25.8%)	0.022
0.7 ML Fe/Mo_2N	0.021 (73.7%)	0.003 (9.5%)	0.005 (16.9%)	0.029
1.1 ML Fe/Mo_2N	0.017 (53.2%)	0.003 (9.3%)	0.012 (37.5%)	0.032
2.0 ML Fe/Mo_2N	0.003 (9.5%)	0.004 (10.6%)	0.026 (79.9%)	0.033
0.4 ML Pt/Mo_2N	0.011 (55.6%)	0.004 (20.2%)	0.005 (25.3%)	0.020
0.7 ML Pt/Mo_2N	0.024 (60.6%)	0.005 (12.6%)	0.012 (30.3%)	0.041
1.3 ML Pt/Mo_2N	0.045 (68.9%)	0.004 (6.1%)	0.017 (26.0%)	0.065
2.1 ML Pt/Mo_2N	0.072 (82.2%)	0.002 (2.3%)	0.014 (16.0%)	0.088

3.1.2. Surface intermediate characterization using vibrational spectroscopy

Vibrational spectroscopic measurements were performed to identify the reaction intermediates on the three types of surfaces. Figure 2 shows the HREEL spectra of Mo_2N, 0.8 ML Fe/Mo_2N and 0.9 ML Pt/Mo_2N surfaces following the adsorption of 5 L isopropanol at 170 K (Figure 2a), and after heating to 350 K (Figure 2b) and 450 K (Figure 2c). The vibrational mode assignments are listed in Table S1. In Figure 2a, the presence of the characteristic vibrational modes of isopropanol and the minimal spectroscopic differences among the three surfaces indicated that isopropanol was molecularly adsorbed at 170 K. A slight shoulder at 3200 cm^{-1} attributed to ν(O−H) of isopropanol was observed, but the corresponding deformation mode, δ(O−H), was not resolved due to the relatively low intensity of this mode for isopropanol.[26,27] The δ(O−H) mode should appear in the spectroscopic region with peaks at 1128 cm^{-1}, 932 cm^{-1}, and 804 cm^{-1}, attributed to the ν_a(C−C−C), ν(C−O), and ν_s(C−C−C) modes, respectively.[26,27]

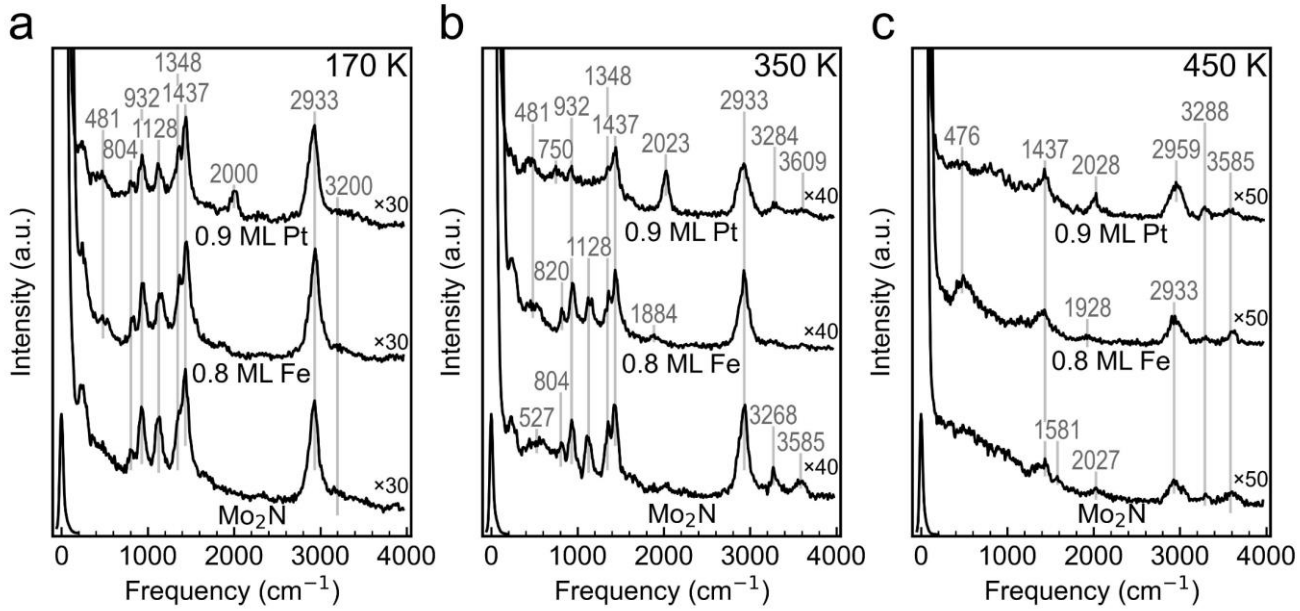

Figure 2. HREEL spectra on Mo_2N, 0.8 ML Fe/Mo_2N, and 0.9 ML Pt/Mo_2N surfaces taken after: (a) exposing the surface to 4 L of isopropanol at 170 K, then (b) flashing the isopropanol-exposed surface to 350 K, then (c) flashing the surface to 450 K.

Upon heating from 170 K (Figure 2b) to 350 K (Figure 2c), the unmodified Mo_2N surface showed minimal spectroscopic changes, suggesting that a significant amount of unreacted isopropanol remained on the surface after the onset of acetone desorption at 350 K. The 350 K spectrum also showed the appearance of two ν(O−H) modes attributed to hydrogen-bonded (3268 cm^{-1}) and isolated (3585 cm^{-1}) hydroxyl groups on the surface, consistent with the high selectivity toward C−O scission that was observed on Mo_2N in TPD measurements. Similarly, minimal changes in the Fe/Mo_2N spectra were observed between these two temperatures. The characteristic ν(C=O) mode of acetone was not observed on any of the surfaces at 260 K (Figure S3a) or 350 K, suggesting that acetone desorbed from the surface as soon as it was produced. The Pt/Mo_2N surface showed significant attenuation of the ν_a(C−C−C), ν(C−O), ν_s(C−C−C), and ρ(CH_3) modes at 350 K, consistent with facile dehydrogenation and detection of the acetone TPD peak centered at 284 K. In addition, the appearance of the γ(CH_2) mode[27] at 750 cm^{-1} suggested that

isopropanol started to decompose and the remaining modes were attributed mainly to hydrocarbon fragments left on the surface.

Figure 2c shows the spectra after heating the surfaces to 450 K. On Mo_2N, most of the characteristic vibrational modes of isopropanol were attenuated by this temperature, suggesting that only hydrocarbon fragments and hydroxyl groups remained on the surface. Significant attenuation of these peaks was also observed on Fe/Mo_2N, in addition to an increase in the ν(Fe−O) mode. Pt/Mo_2N showed minimal changes from 350 K to 450 K, indicating that the decomposition reaction was mostly complete by 350 K.

3.2. Trends in activity on Mo_2N-based powder catalysts

3.2.1. Flow reactor evaluation

In order to extend the findings from UHV to more realistic conditions, the reaction of isopropanol was evaluated in a quartz tube flow reactor over the corresponding supported powder catalysts. CO chemisorption measurements of the prepared catalysts yielded CO uptake values of 6.6 μmol/g on Fe/Mo_2N and 167.7 μmol/g on Pt/Mo_2N, corresponding to 2.6% dispersion of Fe and 65.4% dispersion of Pt. The isopropanol conversion is shown as a function of time-on-stream at the reaction temperatures of 473 K (Figure 3a) and 413 K (Figure 3b), along with the selectivity toward the C_3 products at comparable isopropanol conversions at 413 K (Figure 3c). The main products at steady-state conditions at both temperatures were propylene and acetone, as well as a relatively small amount of propane at 473 K. This temperature was used to compare total conversion of isopropanol on the three catalysts. The initial trend in the conversion correlated well with the total activity that was observed from the TPD studies, in the order of Pt/Mo_2N > Fe/Mo_2N > Mo_2N. At longer reaction times, the Fe/Mo_2N catalyst displayed the most significant deactivation and reached steady-state conversion similar to that for unmodified Mo_2N.

To compare selectivity toward dehydration and dehydrogenation, a lower reaction temperature of 413 K was used. At this temperature, CO formation was not predicted based on thermodynamic analysis. An equilibrium species distribution using the Gibbs energy minimization method in HSC Chemistry predicted 21% isopropanol, 25% propylene, 13% acetone, and 0% CO at 1 atm and 413 K (Figure S4). Therefore, the comparison with the TPD

results was focused on the C_3 dehydration and dehydrogenation products, and not CO. In addition, because the supported powder catalysts possess Fe-Mo_2N and Pt-Mo_2N interfacial sites, the partially covered Fe/Mo_2N and Pt/Mo_2N model surfaces were the most relevant for this comparison.

From Figure 3c, it can be seen that the unmodified Mo_2N displayed the highest propylene production rate (0.42 mmol/h), which corresponded to the highest selectivity toward dehydration (60%), consistent with the maximum C−O scission activity that was observed on the unmodified Mo_2N model surface. For the supported catalysts, metal-modification led to a decrease in the steady-state propylene formation rate to 0.12 mmol/h over Fe/Mo_2N and 0.01 mmol/h over Pt/Mo_2N. This was consistent with the significant attenuation of propylene formation on the Pt/Mo_2N model surface. The Pt/Mo_2N catalyst showed significant deactivation at 413 K, but not at 473 K. This, combined with a comparison of the initial and steady-state product flow rates (Figure S5a) and selectivity (Figure S5b) showing that acetone formation was favored in both cases, suggested that the selectivity could still be compared despite this deactivation. A slight increase in selectivity toward dehydrogenation was observed for Fe/Mo_2N (45.2%) compared to Mo_2N (40%), and the Pt/Mo_2N catalyst was highly selective toward acetone (93.4%). This trend agreed with the observation from the TPD experiments that partially covered Pt/Mo_2N displayed higher acetone activity than Mo_2N or partially covered Fe/Mo_2N surfaces.

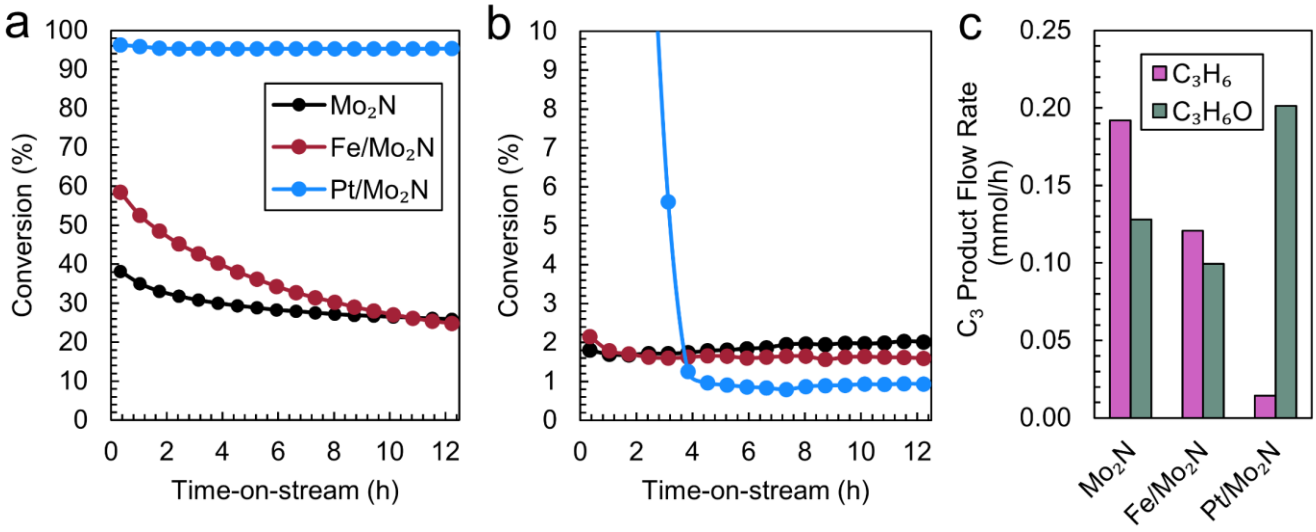

Figure 3. Reaction of isopropanol over Mo_2N (black), Fe/Mo_2N (red), and Pt/Mo_2N (blue) powder catalysts. (a) Conversion at 473 K under equivalent conditions. (b) Conversion of isopropanol at 413 K for the comparison of

selectivity. (c) Steady-state flow rate of the C_3 products, propylene (pink) and acetone (teal), over the three catalysts under comparable conversion (1–2%) at 413 K. The selectivity at 413 K and 473 K is shown in Table S2.

3.2.2. In-situ X-ray absorption measurements

In order to elucidate the oxidation states of the Fe- and Pt-modified Mo_2N catalysts under reaction conditions, in-situ XANES measurements were performed. For Fe/Mo_2N (Figure 4a), the as-synthesized catalyst under N_2 atmosphere at 298 K appeared to be a mixture of metallic Fe^0 and partially oxidized Fe, as suggested by the observation that the peak intensities are between those of the Fe foil and Fe oxides. However, it was found that none of the Fe/Mo_2N spectra could be well-fit by a linear combination of the reference foils and oxides (Table S3 and Figure S6). Under reduction conditions of N_2/H_2 atmosphere at 823 K and during the reaction of isopropanol at 473 K, the peak position shifted slightly to lower energy, suggesting that Fe/Mo_2N might be slightly reduced.

For Pt/Mo_2N (Figure 4b), metallic Pt^0 was the dominant species, as suggested by the observation that the Pt L-edge white line intensity was much closer to that of the Pt foil than PtO_2. While the Pt^0 was the main oxidation state, the Pt in Pt/Mo_2N displayed a stronger white line than the Pt foil, which could be due to the electronic interaction between Pt and Mo_2N. The white line intensity decreased slightly during the reduction and then remained stable during isopropanol reaction at 473 K.

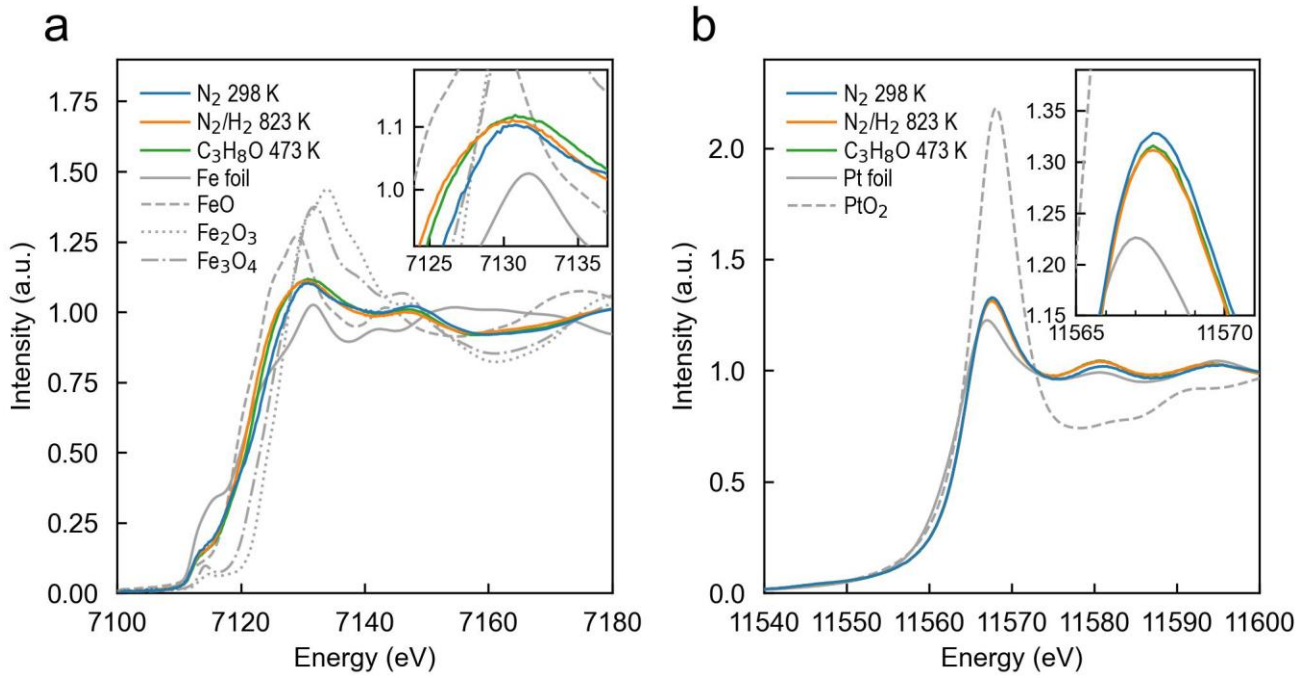

Figure 4. XANES profiles of the Mo_2N-supported powder catalysts as-synthesized (blue) and under reduction (orange) and reaction (green) conditions at the (a) Fe K-edge, (b) Pt L_3-edge. Reference metallic foils and oxides are shown in grey.

3.3. DFT study of reaction mechanisms

To understand the trend in selectivity from preferential dehydration producing propylene to dehydrogenation producing acetone when Pt is deposited on Mo_2N (Figure 1d and Figure 3c), isopropanol reaction on $Mo_2N(111)$ and 1.0 ML $Pt/Mo_2N(111)$ was investigated using DFT. Calculations were performed on Mo_2N, Pt/Mo_2N and Fe/Mo_2N surfaces. However, the Fe monolayer on Mo_2N was not stable and underwent reconstruction after the adsorption of IPA, which made it impossible to obtain accurate binding energy values. Therefore, DFT results will be presented only for the Mo_2N and Pt/Mo_2N surfaces. Upon exposure of $Mo_2N(111)$ to isopropanol, the molecule adsorbs on the top site of Mo through the oxygen moiety ($*CH_3CHOHCH_3$, Figure S8a) with a reaction energy (ΔE) of -0.67 eV (Figure 5a and Table S4). This is followed by the initial dehydrogenation, which prefers the O−H bond scission that leads to the formation of O-anchored isopropoxy in the 3-fold Mo hollow site

(*CH_3CHOCH_3, Figure S8b) (ΔE = -1.44 eV, Figure 5a and Table S4) over the C−H bond scission that leads to the formation of C-/O-co-anchored *CH_3COHCH_3 in the Mo-N bridge site (Figure S8c) (ΔE = -0.08 eV, Figure 5a and Table S4). The preference for alkoxide formation during the decomposition of other alcohols has also been observed on Mo_2N and Mo_2C.[8,28] The adsorbed *CH_3CHOCH_3 then favors the C−O bond scission to form isopropyl (*CH_3CHCH_3, Figure S8e) and *O (Figure S8g) (ΔE = -1.12 eV, Figure 5a and Table S4), resulting in the formation of propylene (*CH_2CHCH_3, Figure S6f) (ΔE = -0.52 eV, Figure 5a and Table S4) as observed experimentally (Figure 3c). Thermodynamically, isopropyl can also be produced via the C−OH bond scission of *$CH_3CHOHCH_3$ on Mo_2N(111), corresponding to a reaction energy of -1.82 eV (Table S4). Although it is thermodynamically more favorable than O−H bond scission, kinetically it is likely more difficult. Previous studies of glycerol decomposition over Mo_2N showed the preference of O−H bond scission over C−OH bond scission.[8] Upon exposure of isopropanol to Mo_2N in our study, the HREEL spectra at reaction temperature also show limited intensity for surface *OH groups and suggest a similar preference to O−H scission (Figure 2). While the C-O bond scission is highly exothermic, the C−H bond scission to form acetone (*CH_3COCH_3, Figure S8d) (ΔE = 0.01 eV, Figure 5a and Table S4) is less competitive on Mo_2N(111), making propylene the major C_3 product.

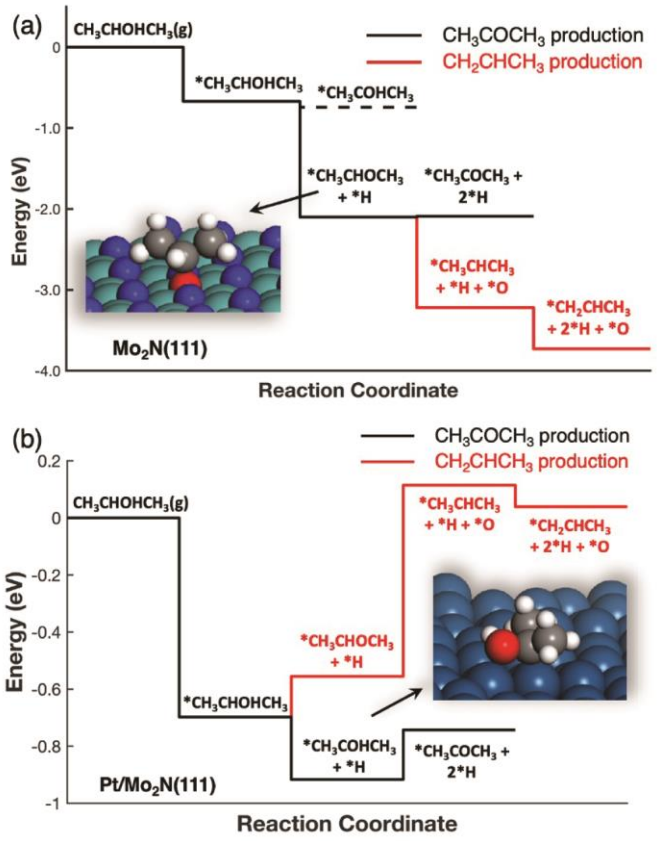

Figure 5. DFT calculated energy profiles of acetone production (black lines) and propylene production (red lines) from isopropanol over (a) $Mo_2N(111)$ and (b) $Pt/Mo_2N(111)$. Insets: DFT optimized structure for (a) $*CH_3CHOCH_3$ on $Mo_2N(111)$, (b) $*CH_3COHCH_3$ on $Pt/Mo_2N(111)$.

Pt-modified Mo_2N behaves differently from Mo_2N. Supported by Mo_2N, the Pt overlayer maintains a very similar geometry (Figure S7b) and electronic structure (Figure 6, blue lines) as seen for Pt(111). As a result, isopropanol decomposes through α C−H bond scission followed by O−H bond scission, similar to the behavior observed for other alcohols on Pt(111) .[29–33] This behavior is distinct from that using common supports like γ-Al_2O_3, where Pt prefers to form 3D nanoparticles as identified in both experimental studies[34] and DFT calculations.[35] Upon the exposure to the $Pt/Mo_2N(111)$ surface, isopropanol adsorbs at the Pt top site of Pt/Mo_2N (Figure S9a) (ΔE = -0.70 eV, Figure 5b and Table S4), and can form either $*CH_3CHOCH_3$ (Figure S9b) or $*CH_3COHCH_3$ (Figure S9c) via the initial dehydrogenation steps. Unlike the $Mo_2N(111)$ surface, the modification of Pt prohibits the formation

of alkoxide (ΔE = 0.14 eV, Figure 5b and Table S4). Instead, the C−H bond scission to produce *CH_3COHCH_3 (ΔE = -0.22 eV, Figure 5b and Table S4) is preferred, where both oxygen and undercoordinated carbon moieties are required for more significant stabilization at the Pt-Pt bridge site. With such preference, the reaction is shifted away from the propylene production, but favoring the acetone production via the subsequent O−H bond scission that leads to the formation of *CH_3COCH_3 (Figure S9d) (ΔE = 0.17 eV, Figure 5b and Table S4). A similar preference for converting hydroxyl groups in alcohols to carbonyl groups has been observed on Pt(111).[29,30,32,36] Note that the C−H bond scission of *CH_3COHCH_3 to *CH_2COHCH_3, the enol tautomer of *CH_3COCH_3, can be an alternative intermediate for the formation of acetone as observed on Pt(111).[37,38]

The tuning of selectivity of isopropanol reaction from propylene as observed for Mo_2N to acetone as observed for Pt/Mo_2N (Figure 1d and Figure 3C) strongly depends on the affinity of active sites to oxygen or species which are only anchored by oxygen. Taking the formation of *CH_3CHOCH_3, a key intermediate that leads to the formation of propylene, for example, previous research of alcohol decomposition on transition metal and transition metal carbide surfaces suggests that the reaction energy of O−H bond scission in alcohols, leading to alkoxide formation, correlates with oxygen binding energy.[28,33,39,40] According to the calculated partial density of states (PDOS, Figure 6), with its delocalized 4d states and a high-lying d band center (-1.12 eV, black line in Figure 6), Mo on the surface of Mo_2N binds oxygen very strongly with (BE(O) = -3.79 eV). In comparison, with lower-lying d band center (-2.65 eV, blue line in Figure 6), Pt on the surface of Pt/Mo_2N shows a much lower oxygen affinity (BE(O) = -1.31 eV). In the case of Mo_2N, such high oxygen affinity contributes to the favored formation of *CH_3CHOCH_3 that is anchored by oxygen only, which leads to the preferred subsequent C−O bond scission and results in the formation of *O and the production of propylene. In the case of Pt/Mo_2N(111), the lower oxygen affinity hinders the formation of alkoxide. On the other hand, to produce acetone, the stabilization of *CH_3COHCH_3 is necessary, which requires both oxygen and carbon anchors and strongly depends on the characteristics of surface sites. It was reported previously that the alkoxide $(CH_3CHOCH_3)^+$ radical is less stable than the $(CH_3COHCH_3)^+$ isomer. [41] Given that, the surface with *CH_3COHCH_3 is ideally more stable than that with *CH_3CHOCH_3. This is the case for Pt/Mo_2N(111), where forming *CH_3COHCH_3 is more favorable than *CH_3CHOCH_3 by 0.36 eV (Table

S4). The Pt overlayer sites are near-neutral and well dispersed in a (111)-like motif, enabling *CH_3COHCH_3 to be anchored by both carbon and oxygen accompanied with considerable electron transfer from Pt (Figure S10). In contrast, on Mo_2N(111), *CH_3COHCH_3 is much less preferred than *CH_3CHOCH_3 by 1.36 eV (Table S4). Mo sites are more positively charged (charge of +1.39 e) than Pt on Pt/Mo_2N(111) (+0.12 e), resulting in the selective interaction with the oxygen moiety of *CH_3COHCH_3 rather than carbon due to the $Mo^{\delta+}$-$C^{\delta+}$ electrostatic repulsion. The carbon of *CH_3COHCH_3 is instead positioned at N sites on the surface via a relatively weaker $N^{\delta-}$-$C^{\delta+}$ attraction. Consequently, the electron transfer primarily from Mo to O helps stabilize *CH_3COHCH_3 (Figure S10).

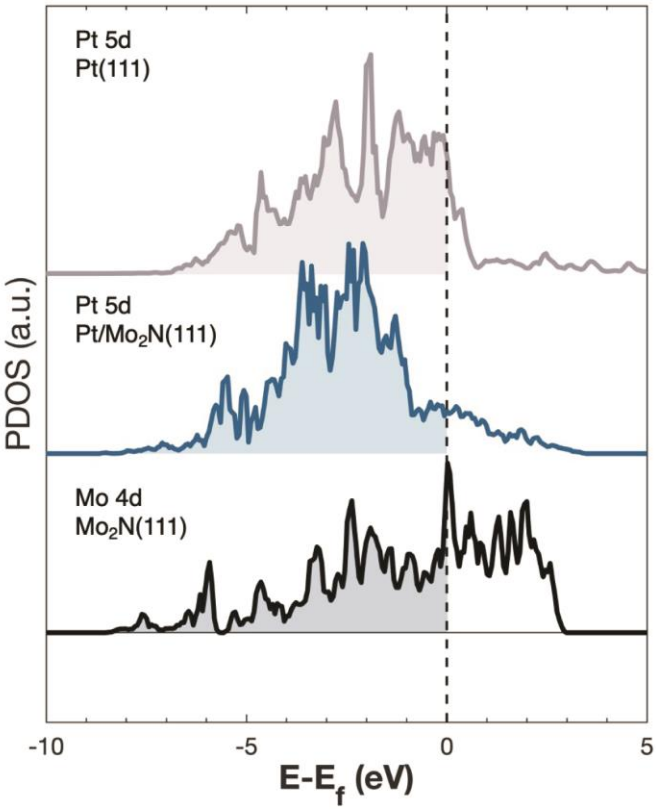

Figure 6. Calculated projected density of states (PDOS) for surface Pt 5d states on Pt(111) surface (gray line), Pt/Mo_2N(111) substrate (blue line), and the Mo 4d states on Mo_2N(111) surface (black line).

4. Conclusions

This work demonstrates the use of model surface studies to guide the design of powder catalysts for selective bond scission reactions using isopropanol as a probe molecule. TPD experiments showed that unmodified

Mo_2N favored propylene formation, and metal modification led to a suppression of dehydration and a promotion of dehydrogenation. Pt/Mo_2N displayed the highest dehydrogenation activity when comparing the partially covered metal-modified surfaces, while Fe-modification did not lead to a significant increase in acetone formation until it reached above-ML coverage. The total activity from the TPD experiments was consistent with the isopropanol conversion observed over corresponding powder catalysts. In addition, a good agreement was observed comparing the trend in acetone production rate on the powder catalysts with that of acetone activity on partially covered model surfaces. In-situ XANES measurements were used to identify the oxidation states of Fe and Pt during the reaction. DFT calculations provided insights into the binding strengths of important intermediates in the dehydration and dehydrogenation pathways on Mo_2N and Pt/Mo_2N, and the origin of the different activity on these surfaces was elucidated through comparison of the PDOS of Mo in Mo_2N with Pt in Pt/Mo_2N. Overall, these results suggested the potential of metal-modified Mo_2N for selective bond scission of isopropanol, and demonstrated the feasibility of using model surface studies to develop supported catalysts.

Acknowledgements

Authors from Columbia University acknowledge support from the United States National Science Foundation DMREF Program under Grant No. CBET1921946. Authors from BNL acknowledge support by the Division of Chemical Sciences, Geosciences, & Biosciences, Office of Basic Energy Sciences, Department of Energy (Grant number DE-SC0012704 with BNL FWP CO-060). Beamline operations at the 7-BM beamline (QAS) at NSLS-II were supported in part by the Synchrotron Catalysis Consortium (U.S. DOE, Office of Basic Energy Sciences, Grant No. DE-SC0012335). DFT calculations in this work were performed using computational resources at Center for Functional Nanomaterials (CFN), and the Scientific Data and Computing Center, a component of the Computational Science Initiative, at Brookhaven National Laboratory under Contract No. DE-SC0012704, and at the National Energy Research Scientific Computing Center (NERSC), a DOE Office of Science User Facility, supported by the Office of Science of the DOE under contract DE-AC02-05CH11231.

References

(1) Chheda, J. N.; Huber, G. W.; Dumesic, J. A. Liquid-Phase Catalytic Processing of Biomass-Derived Oxygenated Hydrocarbons to Fuels and Chemicals. *Angew. Chem. - Int. Ed.* **2007**, *46* (38), 7164–7183. https://doi.org/10.1002/anie.200604274.

(2) Jin, W.; Pastor-Pérez, L.; Shen, D. K.; Sepúlveda-Escribano, A.; Gu, S.; Ramirez Reina, T. Catalytic Upgrading of Biomass Model Compounds: Novel Approaches and Lessons Learnt from Traditional Hydrodeoxygenation – a Review. *ChemCatChem* **2019**, *11* (3), 924–960. https://doi.org/10.1002/cctc.201801722.

(3) Deng, W.; Zhang, Q.; Wang, Y. Catalytic Transformation of Cellulose and Its Derived Carbohydrates into Chemicals Involving C–C Bond Cleavage. *J. Energy Chem.* **2015**, *24* (5), 595–607. https://doi.org/10.1016/j.jechem.2015.08.016.

(4) Lin, Z.; Deshpande, S.; Denny, S. R.; Porter, W. N.; Wang, C.; Marlowe, J.; Christopher, P.; Zheng, W.; Caratzoulas, S.; Vlachos, D. G.; Chen, J. G. Mechanistic Understanding of Ring-Opening of Tetrahydrofurfuryl Alcohol over WO_x-Modified Pt Model Surfaces and Powder Catalysts. *ACS Catal.* **2023**, 8014–8024. https://doi.org/10.1021/acscatal.3c01287.

(5) Liu, W. J.; Yu, H. Q. Thermochemical Conversion of Lignocellulosic Biomass into Mass-Producible Fuels: Emerging Technology Progress and Environmental Sustainability Evaluation. *ACS Environ. Au* **2022**, *2* (2), 98–114. https://doi.org/10.1021/acsenvironau.1c00025.

(6) Requies, J.; Güemez, M. B.; Iriondo, A.; Barrio, V. L.; Cambra, J. F.; Arias, P. L. Biobutanol Dehydrogenation to Butyraldehyde over Cu, Ru and Ru-Cu Supported Catalysts. Noble Metal Addition and Different Support Effects. *Catal. Lett.* **2012**, *142* (1), 50–59. https://doi.org/10.1007/s10562-011-0725-9.

(7) Li, X.; Jia, P.; Wang, T. Furfural: A Promising Platform Compound for Sustainable Production of C_4 and C_5 Chemicals. *ACS Catal.* **2016**, *6*, 7621–7640. https://doi.org/10.1021/acscatal.6b01838.

(8) Lin, Z.; Ammal, S. C.; Denny, S. R.; Rykov, S. A.; You, K.-E.; Heyden, A.; Chen, J. G. Unraveling Unique Surface Chemistry of Transition Metal Nitrides in Controlling Selective C–O Bond Scission Pathways of Glycerol. *JACS Au* **2022**, *2* (2), 367–379. https://doi.org/10.1021/jacsau.1c00403.

(9) Girisuta, B.; Janssen, L. P. B. M.; Heeres, H. J. A Kinetic Study on the Decomposition of 5-Hydroxymethylfurfural into Levulinic Acid. *Green Chem.* **2006**, *8* (8), 701. https://doi.org/10.1039/b518176c.

(10) Huber, G. W.; Iborra, S.; Corma, A. Synthesis of Transportation Fuels from Biomass: Chemistry, Catalysts, and Engineering. *Chem. Rev.* **2006**, *106* (9), 4044–4098. https://doi.org/10.1021/cr068360d.

(11) Wang, T.; Sha, J.; Sabbe, M.; Sautet, P.; Pera-Titus, M.; Michel, C. Identification of Active Catalysts for the Acceptorless Dehydrogenation of Alcohols to Carbonyls. *Nat. Commun.* **2021**, *12* (1), 5100. https://doi.org/10.1038/s41467-021-25214-1.

(12) Yu, Z.; An, X.; Kurnia, I.; Yoshida, A.; Yang, Y.; Hao, X.; Abudula, A.; Fang, Y.; Guan, G. Full Spectrum Decomposition of Formic Acid over γ-Mo_2N-Based Catalysts: From Dehydration to Dehydrogenation. *ACS Catal.* **2020**, *10* (9), 5353–5361. https://doi.org/10.1021/acscatal.0c00752.

(13) Denny, S. R.; Lin, Z.; Porter, W. N.; Artrith, N.; Chen, J. G. Machine Learning Prediction and Experimental Verification of Pt-Modified Nitride Catalysts for Ethanol Reforming with Reduced Precious Metal Loading. *Appl. Catal. B Environ.* **2022**, *312* (December 2021), 121380. https://doi.org/10.1016/j.apcatb.2022.121380.

(14) Yao, S. Y.; Rodriguez, J. Exploring Metal-Support Interactions to Immobilize Sub-Nm Co Clusters on g-Mo2N: A Highly Selective and Stable Catalyst for CO2 Activation. *Abstr. Pap. Am. Chem. Soc.* **2019**, *258*.

(15) Frühberger, B.; Chen, J. G. Reaction of Ethylene with Clean and Carbide-Modified Mo(110): Converting Surface Reactivities of Molybdenum to Pt-Group Metals. *J. Am. Chem. Soc.* **1996**, *118* (46), 11599–11609. https://doi.org/10.1021/ja960656l.

(16) Perdew, J. P.; Burke, K.; Ernzerhof, M. Generalized Gradient Approximation Made Simple. *Phys. Rev. Lett.* **1996**, *77* (18), 3865–3868. https://doi.org/10.1103/PhysRevLett.77.3865.

(17) Blöchl, P. E. Projector Augmented-Wave Method. *Phys. Rev. B* **1994**, *50* (24), 17953–17979. https://doi.org/10.1103/PhysRevB.50.17953.

(18) Kresse, G.; Furthmüller, J. Efficient Iterative Schemes for Ab Initio Total-Energy Calculations Using a Plane-Wave Basis Set. *Phys. Rev. B* **1996**, *54* (16), 11169–11186. https://doi.org/10.1103/PhysRevB.54.11169.

(19) Kresse, G.; Furthmüller, J. Efficiency of Ab-Initio Total Energy Calculations for Metals and Semiconductors Using a Plane-Wave Basis Set. *Comput. Mater. Sci.* **1996**, *6* (1), 15–50. https://doi.org/10.1016/0927-0256(96)00008-0.

(20) Hacene, M.; Anciaux-Sedrakian, A.; Rozanska, X.; Klahr, D.; Guignon, T.; Fleurat-Lessard, P. Accelerating VASP Electronic Structure Calculations Using Graphic Processing Units. *J. Comput. Chem.* **2012**, *33* (32), 2581–2589. https://doi.org/10.1002/jcc.23096.

(21) Hutchinson, M.; Widom, M. VASP on a GPU: Application to Exact-Exchange Calculations of the Stability of Elemental Boron. *Comput. Phys. Commun.* **2012**, *183* (7), 1422–1426. https://doi.org/10.1016/j.cpc.2012.02.017.

(22) Grimme, S.; Antony, J.; Ehrlich, S.; Krieg, H. A Consistent and Accurate *Ab Initio* Parametrization of Density Functional Dispersion Correction (DFT-D) for the 94 Elements H-Pu. *J. Chem. Phys.* **2010**, *132* (15), 154104. https://doi.org/10.1063/1.3382344.

(23) Altarawneh, M.; Jaf, Z.; Oskierski, H.; Jiang, Z.-T.; Gore, J.; Dlugogorski, B. Z. Conversion of NO into N_2 over γ-Mo_2N. *J. Phys. Chem. C* **2016**, *120* (39), 22270–22280. https://doi.org/10.1021/acs.jpcc.6b04107.

(24) Matanović, I.; Garzon, F. H.; Henson, N. J. Electro-Reduction of Nitrogen on Molybdenum Nitride: Structure, Energetics, and Vibrational Spectra from DFT. *Phys. Chem. Chem. Phys.* **2014**, *16* (7), 3014–3026. https://doi.org/10.1039/C3CP54559H.

(25) Bull, C. L.; Kawashima, T.; McMillan, P. F.; Machon, D.; Shebanova, O.; Daisenberger, D.; Soignard, E.; Takayama-Muromachi, E.; Chapon, L. C. Crystal Structure and High-Pressure Properties of γ-Mo_2N Determined by Neutron Powder Diffraction and X-Ray Diffraction. *J. Solid State Chem.* **2006**, *179* (6), 1762–1767. https://doi.org/10.1016/j.jssc.2006.03.011.

(26) Vannice, M. A.; Erley, W.; Ibach, H. A RAIRS and HREELS Study of Isopropyl Alcohol on Pt(111). *Surf. Sci.* **1991**. https://doi.org/10.1016/0039-6028(91)90633-4.

(27) Davis, J. L.; Barteau, M. A. Spectroscopic Identification of Alkoxide, Aldehyde, and Acyl Intermediates in Alcohol Decomposition on Pd(111). *Surf. Sci.* **1990**, *235* (2–3), 235–248. https://doi.org/10.1016/0039-6028(90)90799-E.

(28) Yu, W.; Salciccioli, M.; Xiong, K.; Barteau, M. A.; Vlachos, D. G.; Chen, J. G. Theoretical and Experimental Studies of C−C versus C−O Bond Scission of Ethylene Glycol Reaction Pathways via Metal-Modified Molybdenum Carbides. *ACS Catal.* **2014**, *4* (5), 1409–1418. https://doi.org/10.1021/cs500124n.

(29) Faheem, M.; Saleheen, M.; Lu, J.; Heyden, A. Ethylene Glycol Reforming on Pt(111): First-Principles Microkinetic Modeling in Vapor and Aqueous Phases. *Catal. Sci. Technol.* **2016**, *6* (23), 8242–8256. https://doi.org/10.1039/C6CY02111E.

(30) Liu, B.; Greeley, J. Decomposition Pathways of Glycerol via C–H, O–H, and C–C Bond Scission on Pt(111): A Density Functional Theory Study. *J. Phys. Chem. C* **2011**, *115* (40), 19702–19709. https://doi.org/10.1021/jp202923w.

(31) Sutton, J. E.; Panagiotopoulou, P.; Verykios, X. E.; Vlachos, D. G. Combined DFT, Microkinetic, and Experimental Study of Ethanol Steam Reforming on Pt. *J. Phys. Chem. C* **2013**, *117* (9), 4691–4706. https://doi.org/10.1021/jp312593u.

(32) Gu, X.-K.; Liu, B.; Greeley, J. First-Principles Study of Structure Sensitivity of Ethylene Glycol Conversion on Platinum. *ACS Catal.* **2015**, *5* (4), 2623–2631. https://doi.org/10.1021/cs5019088.

(33) Salciccioli, M.; Chen, Y.; Vlachos, D. G. Density Functional Theory-Derived Group Additivity and Linear Scaling Methods for Prediction of Oxygenate Stability on Metal Catalysts: Adsorption of Open-Ring Alcohol and Polyol Dehydrogenation Intermediates on Pt-Based Metals. *J. Phys. Chem. C* **2010**, *114* (47), 20155–20166. https://doi.org/10.1021/jp107836a.

(34) Okumura, K.; Noda, S. Growth of Pt Crystallites Supported on γ-Al2O3 Studied by Atomic Force Microscopy. *J. Phys. Chem. B* **2001**, *105* (35), 8345–8349. https://doi.org/10.1021/jp010530x.

(35) Li, H.; Wang, H.; Shi, X. Interfacial Parameters of Pt/γ-Al2O3: A First-Principle and MD Simulation Study. *Phys. E Low-Dimens. Syst. Nanostructures* **2020**, *117*, 113804. https://doi.org/10.1016/j.physe.2019.113804.

(36) Salciccioli, M.; Yu, W.; Barteau, M. A.; Chen, J. G.; Vlachos, D. G. Differentiation of O–H and C–H Bond Scission Mechanisms of Ethylene Glycol on Pt and Ni/Pt Using Theory and Isotopic Labeling Experiments. *J. Am. Chem. Soc.* **2011**, *133* (20), 7996–8004. https://doi.org/10.1021/ja201801t.

(37) Jeffery, E. L.; Mann, R. K.; Hutchings, G. J.; Taylor, S. H.; Willock, D. J. A Density Functional Theory Study of the Adsorption of Acetone to the (111) Surface of Pt: Implications for Hydrogenation Catalysis. *Catal. Today* **2005**, *105* (1), 85–92. https://doi.org/10.1016/j.cattod.2005.04.013.

(38) Xu, M.; Huai, X.-L.; Liu, H. Role of Keto–Enol Isomerization on Surface Chemistry and Hydrogenation of Acetone on Pt(111): A DFT Study. *Ind. Eng. Chem. Res.* **2014**, *53* (13), 5451–5454. https://doi.org/10.1021/ie404080x.

(39) Salciccioli, M.; Vlachos, D. G. Kinetic Modeling of Pt Catalyzed and Computation-Driven Catalyst Discovery for Ethylene Glycol Decomposition. *ACS Catal.* **2011**, *1* (10), 1246–1256. https://doi.org/10.1021/cs2003593.

(40) Salciccioli, M.; Vlachos, D. G. Kinetic Modeling of Pt-Catalyzed Glycolaldehyde Decomposition to Syngas. *J. Phys. Chem. A* **2012**, *116* (18), 4621–4628. https://doi.org/10.1021/jp3017216.

(41) Nobes, R. H.; Radom, L. Structures and Relative Energies of Gas Phase [C3H7O]+ Ions. *Org. Mass Spectrom.* **1984**, *19* (8), 385–393. https://doi.org/10.1002/oms.1210190807.